Grid-Forming Converter Current Limiting Design to Enhance Transient Stability for Grid Phase Jump Events

Xianxian Zhao, Damian Flynn

School of Electrical and Electronic Engineering, University College Dublin, Dublin 4, D04 V1W8 Republic of Ireland (Tel: +35317161959; e-mail: xianxian.zhao@ucd.ie)

Abstract: Grid-forming converters (GFs) are seen as a replacement for synchronous machines in future power systems. Compared with synchronous machines, GFs provide much reduced overcurrent capability and hence they experience current saturation more frequently for the same capacity. Moreover, once in current saturation, GFs have limited regulation capability, and can become unstable if the current limiting control is improperly designed. Hence, in order to enhance GF stability when subject to phase jump down disturbances and current saturation, a combination of virtual impedance (VI) current limiting and scaling current reference saturation control is proposed. A relatively large virtual reactance-resistance ratio is also recommended. To speed up GF recovery, an (increased) transient P/f droop gain is proposed for downward phase jumps, but not fault conditions. Simulation studies on a simple system under large phase-jump events, i.e. ±60°, confirm the effectiveness of the proposed approach.

Keywords: Grid-forming converters, virtual impedance current limiting control, current saturation, phase jump disturbances, synchronous machines, transient stability.

1. INTRODUCTION

To reduce carbon emissions and combat climate change, converter-based variable renewable energy generation, mainly from wind and photovoltaic (PV) energy sources, are rapidly replacing traditional synchronous machine-based fossil fuel energy generation in power systems around the world (Hodge et al., 2020). Existing power converters are predominantly controlled as "grid-following", since they can precisely follow a power reference, which supports maximum power capture in wind and PV energy generation systems, and for maintaining the DC link voltage in high voltage direct current transmission and static reactive power compensation systems. Consequently, grid-following converters (GLs) need to be synchronized to the grid voltage angle using phase-locked loop (PLL) techniques (Zhao et al., 2022). Thus, when the GL share increases beyond some point, the grid is no longer able to provide a "stiff" voltage for them to follow and provide stable outputs (Zhao and Flynn, 2022).

Controlling some voltage source converters using a "grid-forming" mode has previously been proposed to support system stability, while also considering increased use of battery storage (Zhao et al., 2021a) and high voltage direct current transmission. Grid-forming converters (GFs) create their own internal voltage angle, such that they can provide a voltage reference for GLs. The ability to create a voltage output, and an inherent inertial response, makes GFs similar to synchronous machines, such that they can provide an immediate respond to voltage and frequency disturbances. Moreover, GFs can also provide blackstart capability, which further sees them as offering a long-term replacement for synchronous machines in future power grids.

Compared with synchronous machines, GFs offer much faster and more flexible controllability. However, once in current saturation, their regulation capability is greatly reduced, and they can go unstable without careful design of the current limiting control. In addition, since a GF has much less overcurrent capability than a synchronous machine (typically 20% of its rated current versus up to seven times for a synchronous machine), GFs will tend to be in a current limited state much more often than synchronous machines of the same capacity (Denis et al., 2018). Traditionally, transient stability is defined as the ability to maintain synchronism when subject to severe transient disturbances, such as faults on transmission facilities, loss of generation or a large load (Kundur, 1994). Here, transient stability for a GF is defined as, when subject to current saturation, its ability to maintain synchronism and provide acceptable output power and voltage support under transient disturbances. The key difference is that the transient disturbances need not be that severe to cause GF current saturation.

GF transient stability under fault conditions, based on the above definition, has been analysed, using, for example, power-angle relationship (Huang et al., 2017, Qoria et al., 2019, Rokrok et al., 2021) and Lyapunov's direct method (Shuai et al., 2018). Stability enhancement methods which involve reducing fault-induced acceleration of the generated internal voltage angle have also been proposed in Qoria et al. (2019), Shuai et al. (2018), Huang et al. (2017), Xiong et al. (2021), Eskandari and Savkin (2020), Zhao and Flynn (2020, 2022). In Rokrok et al. (2021), the current reference angle is also shown to impact GF transient stability with only current reference saturation control, i.e. directly limiting the current references, which can be interpreted as showing the impact of the d- and q-axis components of the GF internal voltage.

Although GF transient stability under fault conditions has been widely and extensively studied, less focus has been placed on investigating GF performance under phase jumps (not due to low voltage faults) while being subject to current saturation. Phase jumps are usually linked to line tripping, system splits, large load sudden dis- and re-connections. In Rokrok et al. (2021), a power-angle relationship schematic is used to analyse GF transient stability under phase jumps. However, the GF is only under current reference saturation control, with a fixed assigned current reference angle, which causes the GF to easily go unstable for downward phase jumps, seen as high-frequency power output oscillations. In Qoria et al. (2019), based on numerical simulations, slowing down changes in the generated internal voltage angle help to extend GF recovery. In general, existing analysis and enhancement methods for GF transient stability under fault conditions may not be applicable for phase jumps. For example, for a downward phase jump a GF should increase its active power output to maintain stability, while during a fault the GF active power output is normally reduced, while after the fault is cleared the power output may be higher or lower than the reference. Phase jumps are not traditionally studied, since synchronous machines have large overcurrent capability, but for systems with large GF/GL shares, the reduced overcurrent capability raises concerns. Assuming that the GF active power reference has a positive value, the main contributions of this paper are summarized as follows:

- GF transient stability, under various current limiting controls, for both up/down phase jumps under different operational conditions is investigated.
- Combined virtual impedance (VI) current limiting and scaling current reference saturation control is proposed to enhance GF transient stability for downward phase jumps. In addition, combined VI and d-axis current priority current reference control is shown to negatively affect GF ability to exit current saturation and ensure stability.
- High virtual reactance-resistance ratio, $\sigma_{X/R}$, can enhance GF transient stability under downward phase jump (i.e. stability is retained with a weaker grid and higher initial current), but they can excite high-frequency power output oscillations for a strong grid.
- A high gain transient P/f droop during a downward phase jump down can accelerate GF recovery.

The paper is organized as follows: droop control-based grid-forming converter modelling, and proposed current limiting control and P/f droop gain design are described in Section 2; simulation results for up/down phase jumps for varying network conditions are then presented in Section 3; finally, Section 4 concludes the paper.

2. GRID-FORMING CONVERTER CURRENT LIMITING CONTROL FOR PHASE JUMP EVENTS

A droop control-based grid-forming converter with inner cascaded voltage and current PI control is first described, before the proposed combination of virtual impedance current limiting and scaling-based current reference saturation control is introduced. Finally, in order to accelerate GF post-disturbance recovery a modified P/f droop is investigated.

2.1 Grid-forming converter model with inner cascaded voltage and current PI control loops

A voltage source converter with a PI-controlled DC current source, capacitor and LCL filter, connecting to an AC grid, is shown in Fig. 1. The DC current source represents DC-side input power, such as from a PV panel, wind turbine or energy storage. The AC grid is represented by an ideal voltage source in series with an impedance (R_g, L_g). A step-up

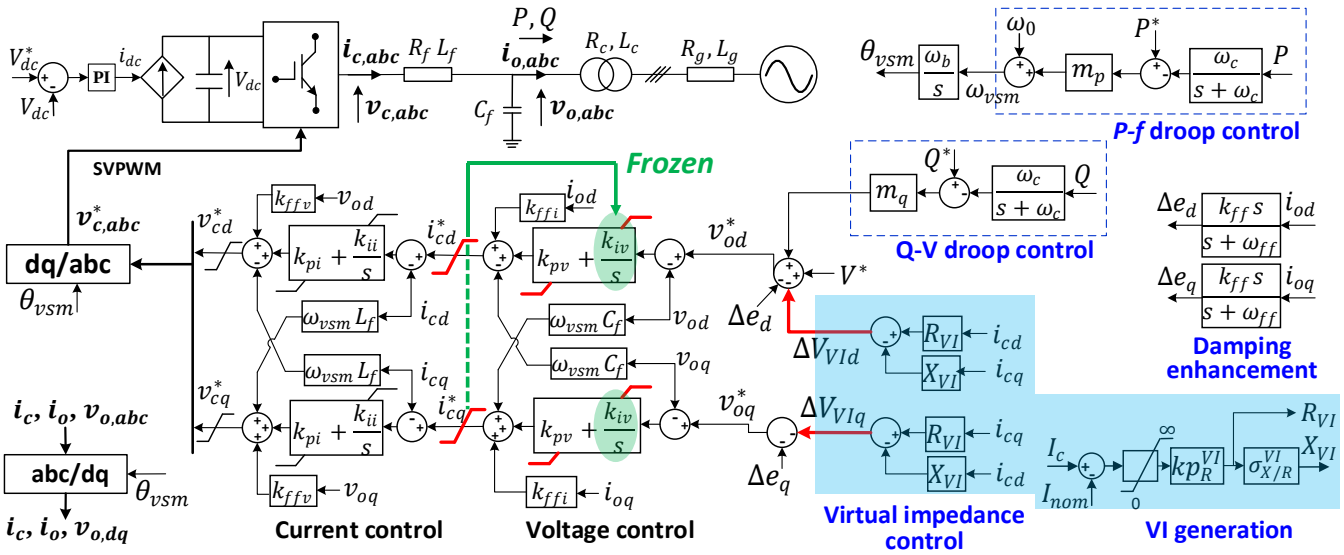

Parameter	Value (pu)	Parameter	Value (pu)
R_f, L_f, C_f,R_c, L_c	0.005, 0.15, 0.066, 0.005, 0.15	k_{pv}, k_{iv}, k_{pi}, k_{ii}	0.52, 1.161022, 0.7388, 1.19
m_p, m_q, ω_0	0.02, 0.0001, 1	$i_c^* = (i_{cd}^{*2} + i_{cq}^{*2})^{0.5}$	≤ 1.25
K_{ffi}, K_{ffv}, ω_{ff}, K_{ff}	1, 1, 16.66, 0.01	kp_{RVI}, $\sigma_{X/R}$, I_{nom}	0.67, 5, 1
V_{dc}^*, V^*, Q^*	1, 1, 0	C_{dc}, K_p^{dc}, K_i^{dc}	2 mF, 82, 2048

Figure 1. Droop control-based GF connected to a DC current source and an AC grid via a LCL filter, and its control structure and parameters.

transformer, R_c, L_c, represents the grid-side L filter. Fig. 1 also shows a droop control-based GF control structure, with cascaded voltage and current PI control loops. The P/f droop control generates the converter internal voltage angular speed ω_{vsm} and angle θ_{vsm}. The Q/V droop control generates the voltage deviation ΔV (whose impact can be ignored since the droop gain m_q is small), which is then added to V^* to form the d-axis output voltage reference, v_{od}^*. The q-axis output voltage reference v_{oq}^* is set as zero. Thus, the dq coordinates employed for the decoupling control rotate at speed ω_{vsm}, with the d-axis aligned with the internal / output voltage. The cascaded voltage and current PI control structure is adopted here, as it ensures full use of the LC filter dynamics to realize the GF control requirements and current limitation. The PI controller parameters follow Qoria et al. (2018), which are tuned to provide the largest damping ratio for a GF connected to a grid with a high short-circuit ratio (corresponding to a worst case scenario). Damping enhancement control (Δe_d, Δe_q) is also added to the output voltage references, v_{od}^*, v_{oq}^*.

Threshold virtual impedance current limiting is also shown in Fig. 1, whereby if the measured converter current magnitude, I_c, exceeds I_{nom} the virtual resistance and reactance, $R_{VI} > 0$ & $X_{VI} > 0$, and the VI control are activated. The generated dq axis voltage drop, ΔV_{VId}, ΔV_{VIq}, are then added to v_{od}^* and v_{oq}^*. In Fig. 1, only a schematic of the current reference saturation control is shown. Fig. 2 shows the scaling current reference saturation control, such that when $i_c^{*0} \geq I_{max}$, i_{cd}^{*0} and i_{cq}^{*0} are scaled down to make $i_{cd}^{*2} + i_{cq}^{*2} \leq I_{max}^2$, and, in addition, the integrator of the outer PI controller is frozen by setting its input to zero. Other strategies can achieve the same mathematical relationship, $i_{cd}^{*2} + i_{cq}^{*2} \leq I_{max}^2$, e.g. d- or q-axis current prioritization (detailed in Zhao and Flynn (2020, 2022)), or $i_{cd}^* = I_{max}\cos(\theta)$, $i_{cq}^* = I_{max}\sin(\theta)$, and θ is a fixed angle as in Rokrok et al. (2021).

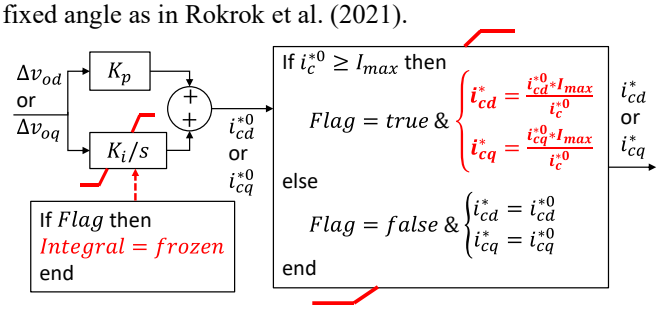

Figure 2. Scaling current reference saturation control including anti-windup integration in the outer voltage PI control, where i_{cd}^{*0} and i_{cq}^{*0} are the d- and q-axis current references from the outer voltage control loop, and i_c^{*0} is the relevant amplitude.

2.2 Proposed combination of virtual impedance and scaling-down currant limiter for grid-forming converters

The following proposals are based on the simulation results presented in Section 3, rather than mathematical analysis, since once a GF is in current limitation, the current limiting controls being employed dominate the GF dynamic stability, and as the current limiting control uses current (or current reference) amplitude as input, the GF modelling is nonlinear.

1) Combination of VI current limiting and scaling current reference saturation control: The grid-forming converter in Fig. 1 with only current reference saturation control easily loses stability or outputs high-frequency power oscillations following a large downward phase jump disturbance. Such difficulties can be avoided using "soft" VI current limiting control, since when the virtual impedance is activated, the outer voltage PI control operates as normal, and, hence, the output voltage can be directly controlled. However, using only VI control, the initial converter fault current is high and takes ≈20 ms to die away. Consequently, a combination of VI and scaling current reference saturation control is proposed. VI control tends to dominate the GF dynamics, while scaling current reference control only tends to limit the current during the initial transients, since the scaling approach acts in proportion to the current magnitude. In comparison with the current reference saturation strategy in Rokrok et al. (2021), scaling avoids the need to define a fixed current reference angle which ensures GF stability.

2) Selection of virtual reactance-resistance ratio, $\sigma_{X/R}$: In Paquette and Divan (2014), small-signal analysis showed that a sufficiently large $\sigma_{X/R}$ can ensure good GF damping during overcurrent conditions. Here, large-signal simulations show that a sufficiently large $\sigma_{X/R}$ can, on the one hand, ensure that a GF rides through a downward phase jump under weak grid conditions, or a phase jump of greater magnitude. However, on the other hand, a high $\sigma_{X/R}$ can result in high-frequency output power oscillations when connected to a strong grid. In practice, a reasonably large $\sigma_{X/R}$ is preferred, since high-frequency oscillations can be readily filtered out. With $\sigma_{X/R}$ chosen, the proportional gain kp_{RVI} is selected by ensuring that the converter steady-state current is limited to I_{maxVI} when a bolted 3-phase fault is applied at the C_f output node.

3) Transient P/f droop gain during downward phase jumps to accelerate GF recovery: Fig. 3 shows the proposed design for the droop gain, m_p, which increases to m_{p1} if $R_{VI} \geq \varepsilon$ (i.e. VI control is activated), and the output voltage V and active power P are not each lower than V_l and P_l. The OR logic in Fig. 3 avoids m_p being increased to m_{p1} during faults, as demonstrated in Zhao and Flynn (2020), since a smaller m_p can enhance GF stability under faults by slowing down any change in the virtual angle, θ_{vsm}.

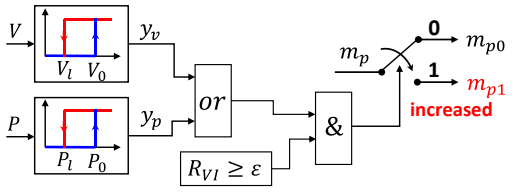

Figure 3. Proposed P/f droop gain m_p to accelerate GF recovery for downward phase jumps. V_0 and P_0 are the pre-event output voltage and active power, V_l and P_l are lower limits (here set $V_0 - 0.25$ pu and $P_0 - 0.2$ pu), $\varepsilon = 0.02$ pu, and $m_{p1} = 3m_{p0} = 0.06$.

3. CASE STUDIES AND RESULTS

The system shown in Fig. 1 is simulated to investigate grid-forming stability for different current limiting strategies for up/down phase jumps, assuming different grid strengths, transmission line characteristics and active power references. The VI control is activated when $I_c \geq 1$ pu, and the default

values for kp_{RVI} and $\sigma_{X/R}$ are 0.67 and 5, respectively, following Qoria et al. (2018). I_{maxVI} is set at 1.2 pu, while I_{max} for current reference saturation control is 1.25 pu, as indicated in Fig. 1. The simulation studies are performed using Dymola software, using Dassl numerical integration algorithm with step size of 0.01 ms.

3.1 Grid-forming stability assessment with different current limiting control for upward phase jumps

A +60° phase jump is applied at 2 s to the AC grid in Fig. 1, with GF stability investigated under VI, id priority, and scaling current reference saturation control. P^* is set high at 0.95 pu. R_g and L_g are 0.045 pu and 0.35 pu, respectively. The simulation results are shown in Fig. 4, which indicate that the GF quickly returns to its pre-event state in a similar manner for all control approaches, even with such high P^*. In each case the converter current is quickly reduced after an initial transient peak during the upward phase jump, as seen in Fig. 4(d). It follows that GF stability under upward phase jumps is of little concern.

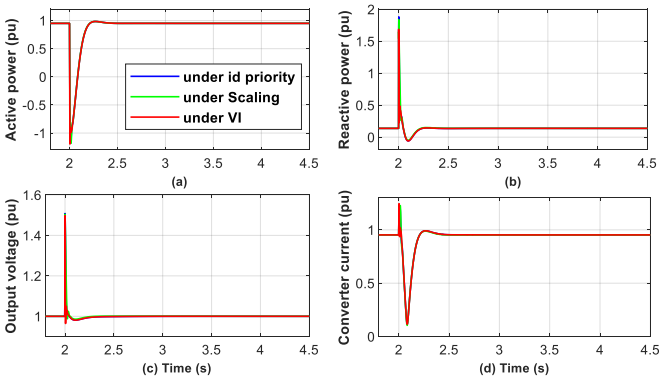

Figure 4. GF dynamic performance under different current limiting control for an upward 60° phase jump.

3.2 Grid-forming transient stability assessment with different current limiting control for downward phase jumps

A downward 60° phase jump down is now applied at 2 s to the AC grid, and Cases 1–5 are defined for different current limiting strategies (Table 1) with $P^* = 0.8$ pu. R_g and L_g remain unchanged for all cases. The simulation results for Cases 1–5 are shown in Fig. 5, which indicate that only under Cases 3 and 5 is the system stable, depending on whether the active power is lower than (or even negative) the pre-event value during the phase jump period, as seen in Fig. 5(b). Now looking at the unstable cases, Fig. 5(b) shows that for cases 1 and 4 that the reactive power output increases to a high value without recovery, leading to a high voltage, as seen in Fig. 5(c). Fig. 5(b)(c) also show that for case 2 that the reactive power and voltage exhibit high values before returning to their pre-event states. For the unstable cases, the initial voltage in Fig. 5(c) falls as low as 0.35 pu, while for the stable cases the initial voltage remains above 0.75 pu. Fig. 5(d) also shows that for Cases 1 and 4 that the converter current remains in saturation after the phase jump occurs.

From the above analysis it follows that, with reference to the unstable case 2, that the converter becomes stable under Case 5 once VI control is added, while, in comparison with Case 1, the GF remains unstable under Case 4 (GF dynamics are very similar). Here, although VI control has been added under Case 4, the id priority current reference saturation limiter severely impacts the d- and q-axis current references once the converter enters current saturation, such that VI control has little effect on GF stability. From the sub-figure in Fig. 5(d), the current under Cases 1, 2, 4 and 5 is immediately limited to I_{max}, 1.25 pu, while under Case 3 the current reaches as high as 1.55 pu and takes ≈20 ms to settle down to I_{maxVI}, 1.2 pu. For Cases 1 and 2 with only current reference saturation control applied, the current is not immediately restricted to I_{max} but instead takes ≈1.5 ms to settle, which is due to the emulated delay (0.2 ms) for the current and voltage measurements. The amplitude of the current oscillations under Case 5 are much reduced compared to Case 3, although the duration is extended compared to Case 2. In summary, for severe downward phase jumps, it can be concluded that:

(a) Stability is quickly lost with "hard" current reference saturation control;
(b) VI control enables stability, but the initial current is high with oscillations lasting for ≈20 ms;
(c) The combination of VI and id priority current reference saturation control leads to instability; and
(d) The proposed combination of VI and scaling current reference saturation control results in GF stability and effective limitation of the current.

Table 1. Simulation settings for Cases 1 – 5

Case 1	Case 2	Case 3	Case 4	Case 5
id priority	Scaling	Virtual impedance	id priority + VI	Scaling + VI

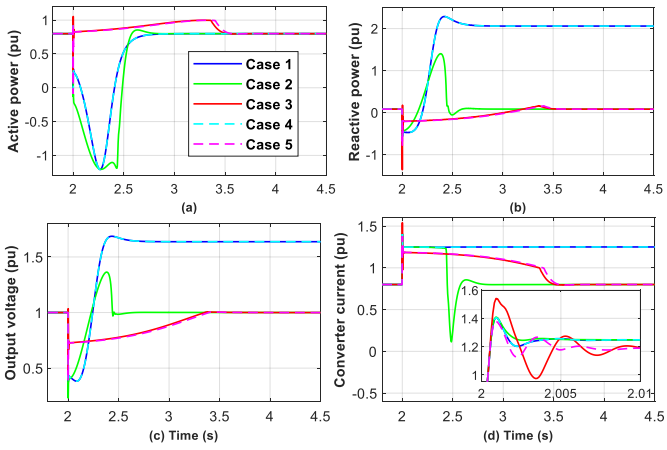

Figure 5. Cases 1 – 5 for different GF current limiting control under a downward 60° phase jump.

Case 6: The GF is now operated under the current limiting method presented in Rokrok et al. (2021), with θ chosen as –30°. The remaining settings are the same as Cases 1 – 5. From Fig. 6(a)(b) it follows that the GF can be stabilized if the current reference angle, θ, is well chosen, but high-frequency oscillations can be excited. Note that the oscillations are not due to numerical instability arising from the implementation of the outer voltage anti-windup PI block, or the choice of numerical integration algorithm, since they also occur when the outer voltage integrator is removed, or

when alternative numerical integration algorithms are employed, e.g. 4th/5th order single-step/Runge Kutta method with fixed/variable step size.

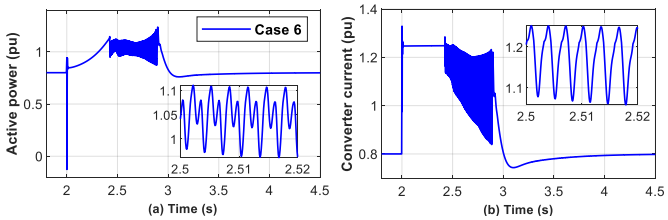

Figure 6. Case 6 for GF current limiting control method in Rokrok et al. (2021), $i_{cd}^{*} = I_{max}\cos(\theta)$, $i_{cq}^{*} = I_{max}\sin(\theta)$, and $\theta = -30°$, for a downward 60° phase jump.

3.3 Grid-forming transient stability enhancement under downward phase jumps

1) Using larger $\sigma_{X/R}$ ratio: Based on Case 5, Cases 7–10 for different network connections (shown in Table 2) are now simulated. The "weaker grid" is achieved by increasing R_g, L_g from 0.045 pu and 0.35 pu to 0.05 pu and 0.5 pu, while the "Distribution grid" involves adjusting the grid impedance ratio, σ_{X_g/R_g}, from 8 to 3, while ensuring that the total impedance is unchanged from the "Weaker grid" case, and, finally, "Larger $\sigma_{X/R}$" involves VI $\sigma_{X/R}$ being increased from 5 to 12.5 (with k_{pRVI} changed from 0.67 to 0.27).

The simulation results for Cases 7–10 are shown in Fig. 7. In comparison to Case 5, the previously stable system now goes unstable for the weaker grid conditions of Case 7, while under Case 8, more closely representing a distribution line, the system now stabilizes. Increasing the $\sigma_{X/R}$ ratio in conjunction with VI control, Case 9, also makes the converter stable, while further assuming a distribution line, in Case 10, speeds up the system recovery. Fig. 7(a) shows that for the stable cases, 8–10, that the initial active power is higher than the pre-event value, while for the unstable case 7 it is lower, similar to the observations for Cases 1, 2 and 4. The output reactive power in Fig. 7(b) closely follows the output voltage in Fig. 7(c), while Fig. 7(c) also indicates that the higher the initial voltage, the faster the GF recovers. Fig. 7(d) shows that the converter current is quickly limited to 1.25 pu and reduced within 1.2 pu, similar to Case 5, due to the proposed combination of VI and scaling current reference control. In summary, for downward phase jumps it follows that:

(a) stability is reduced under weaker grid conditions;
(b) distribution network connections support stability; and
(c) stability is improved with a higher virtual impedance ratio, $\sigma_{X/R}$.

Table 2. Based on Case 5, simulation settings for Cases 7 – 10

	Weaker grid	Distribution grid	larger $\sigma_{X/R}$
Case 7	Yes		
Case 8	Yes	Yes	
Case 9	Yes		Yes
Case 10	Yes	Yes	Yes

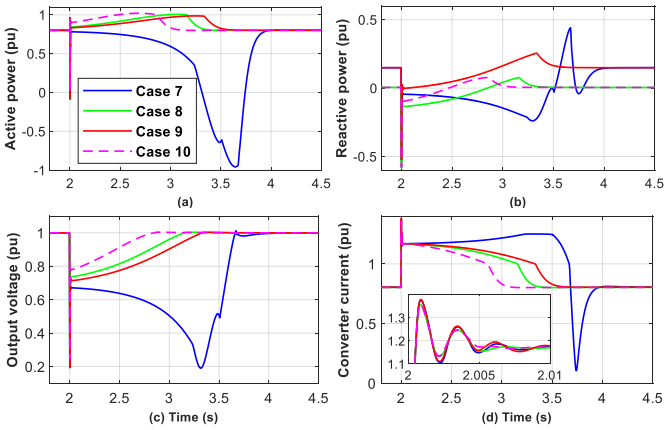

Figure 7. Cases 7–10, based on Case 5, with a combination of a weaker AC grid, distribution line, and/or larger VI $\sigma_{X/R}$.

2) Using proposed droop gain m_p for downward phase jump: Based on Case 5, Cases 11–14 (shown in Table 3) are simulated. Relative to Case 5, "Higher P^*" means that P^* is changed from 0.8 pu to 0.85 pu, "Transient m_p" indicates that the control logic of Fig. 3 is implemented, while "Larger $\sigma_{X/R}$" requires that $\sigma_{X/R}$ increases from 5 to 12.5. Fig. 8 indicates that the system goes unstable in Case 11 with a higher P^*, since the pre-event current is already high (the GF is also unstable if P^* is unchanged from Case 5 but the pre-event reactive power is higher. If the transient droop is activated, Case 12, the GF is still unstable, but returns to pre-event conditions more quickly. Finally, the GF is stabilized in Case 13, with a larger $\sigma_{X/R}$, while again activating the transient droop in Case 4 achieves a faster recovery.

(a) Cases 11, 13 and 14 again confirm that a higher virtual impedance ratio $\sigma_{X/R}$ allows the GF to operate at a higher current output prior to a downward phase jump.
(b) Cases 11, 12 and 14 show that a transient droop, m_p, can improve the recovery time for a stable GF, but cannot enhance GF stability itself for downward phase jumps.

3) Impact of large VI $\sigma_{X/R}$ for a strong grid: Based on Case 13, the GF is now connected to a very strong grid (i.e. L_g is reduced from 0.35 pu to 0.05 pu while σ_{X_g/R_g} is unchanged), as summarized in Table 3. Fig. 9 shows that the GF in Case 15 returns to its initial state more quickly, but the output power and current reveal larger and more sustained high-frequency oscillations (from < 20 ms to > 80 ms). It follows that selecting $\sigma_{X/R}$ should be carefully balanced between ensuring GF stability and avoiding high-frequency power and current oscillations.

Table 3. Based on Case 5, simulation settings for Cases 11 – 15

	Higher P^*	Transient m_p	Larger $\sigma_{X/R}$	Very strong grid
Case 11	Yes			
Case 12	Yes	Yes		
Case 13	Yes		Yes	
Case 14	Yes	Yes	Yes	
Case 15	Yes		Yes	Yes

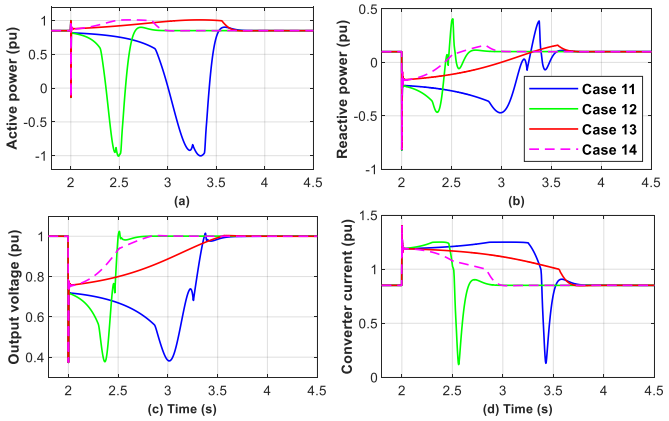

Figure 8. Cases 11 – 14, based on Case 5, with combination of higher P^*, using larger m_p, and/or larger VI $\sigma_{X/R}$.

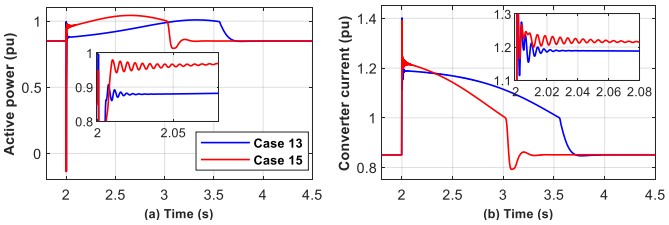

Figure 9. Cases 13 and 15, where, for Case 15, a larger $\sigma_{X/R}$ and much stronger grid condition are considered.

4. CONCLUSIONS

GF stability in relation to phase jump disturbances combined with current saturation rarely has received limited attention. For upward phase jumps, there is little of concern for GF stability, as the GF will not be in current saturation. However, for downward phase jumps, a combination of VI current limiting and scaling current reference saturation control, with a relatively large virtual impedance $\sigma_{X/R}$ was proposed to enhance GF stability. In order to speed up GF recovery, the P/f droop gain, m_p, was also transiently increased. The effectiveness of the proposals was validated under simulation studies on a simple system under large grid phase jumps, i.e. ±60°. Recognising that phase jumps are an emerging concern, work is in progress regarding assessing the likelihood and severity of such events, and the effectiveness and associated cost of various mitigation options, including increased converter current limits.

ACKNOWLEDGEMENTS

Xianxian Zhao is supported by Science Foundation Ireland under Investigator Award SFI/15/IA/3058.

REFERENCES

Denis, G., Prevost, T., Debry, M., Xavier, F., Guillaud, X. & Menze, A. 2018. MIGRATE project: challenges of operating a transmission grid with only inverter - based generation. A grid - forming control improvement with transient current - limiting control. *IET Renewable Power Generation,* 12, 523-529.

Eskandari, M. & Savkin, A. V. 2020. On the impact of fault ride-through on transient stability of autonomous microgrids: nonlinear analysis and solution. *IEEE Transactions on Smart Grid,* 12, 999-1010.

Hodge, B., Jain, H., Brancucci, C., Seo, G., Korpas, M., Kiviluoma, J., Holttinen, H., Smith, J., Orths, A. & Estanqueiro, A. 2020. Addressing technical challenges in 100% variable inverter - based renewable energy power systems. *Wiley Interdiscipl. Reviews: Energy and Environment,* 9, e376.

Huang, L., Xin, H., Wang, Z., Zhang, L., Wu, K. & Hu, J. 2017. Transient stability analysis and control design of droop-controlled voltage source converters considering current limitation. *IEEE Transactions on Smart Grid,* 10, 578-591.

Kundur, P. 1994. *Power system stability and control*, New York: McGraw-Hill.

Paquette, D. and Divan, M. 2014. Virtual impedance current limiting for inverters in microgrids with synchronous generators. *IEEE Transactions on Industry Applications,* 51, 1630-1638.

Qoria, T., Cossart, Q., Li, C., Guillaud, X., Colas, F., Gruson, F. & Kestelyn, X. 2018. Deliverable 3.2: Local control and simulation tools for large transmission systems. *MIGRATE project*.

Qoria, T., Gruson, F., Colas, F., Denis, G., Prevost, T. & Guillaud, X. 2019. Critical clearing time determination and enhancement of grid-forming converters embedding virtual impedance as current limitation algorithm. *IEEE Journal of Emerging and Selected Topics in Power Electronics,* 8, 1050-1061.

Rokrok, E., Qoria, T., Bruyere, A., Francois, B. & Guillaud, X. 2021. Transient stability assessment and enhancement of grid-forming converters embedding current reference saturation as current limiting strategy. *IEEE Transactions on Power Systems*.

Shuai, Z., Shen, C., Liu, X., Li, Z. & Shen, Z. J. 2018. Transient angle stability of virtual synchronous generators using Lyapunov's direct method. *IEEE Transactions on Smart Grid,* 10, 4648-4661.

Xiong, X., Wu, C., Cheng, P. & Blaabjerg, F. 2021. An optimal damping design of virtual synchronous generators for transient stability enhancement. *IEEE Transactions on Power Electronics*.

Zhao, F., Wang, X., Zhou, Z., Harnefors, L., Svensson, J. R. & Gryning, M. 2021a. Control interaction modeling and analysis of grid-forming battery energy storage system for offshore wind power plant. *IEEE Transactions on Power Systems*.

Zhao, X. & Flynn, D. 2020. Freezing grid-forming converter virtual angular speed to enhance transient stability under current reference limiting. *IEEE 21st Workshop on Control and Modeling for Power Electronics*, 1-7.

Zhao, X., Thakurta, P. & Flynn, D. 2022. Grid - forming requirements based on stability assessment for 100% converter - based Irish power system. *IET Renewable Power Generation*, 16(3), 447-458.

Zhao, X. & Flynn, D., 2022. Stability enhancement strategies for a 100% grid - forming and grid - following converter - based Irish power system. *IET Renewable Power Generation*, 16(1), 125-138.